Journal of Solid State Chemistry 182 (2009) 2344–2349

Contents lists available at ScienceDirect

Journal of Solid State Chemistry

journal homepage: www.elsevier.com/locate/jssc

Phases in the Al–Yb–Zn system between 25 and 50 at% ytterbium

Donata Mazzone [a], Pietro Manfrinetti [b,c], Maria L. Fornasini [b,*]

[a] INSTM and Sezione di Chimica Inorganica, Dipartimento di Chimica e Chim. Ind., Università di Genova, Via Dodecaneso 31, 16146 Genova, Italy
[b] Sezione di Chimica Fisica, Dipartimento di Chimica e Chim. Ind., Università di Genova, Via Dodecaneso 31, 16146 Genova, Italy
[c] LAMIA Laboratory-CNR-INFM, Corso Perrone 24, 16152 Genova, Italy

ARTICLE INFO

Article history:
Received 25 March 2009
Received in revised form
1 June 2009
Accepted 6 June 2009
Available online 12 June 2009

Keywords:
Crystal structure
Aluminium
Ytterbium
Zinc

ABSTRACT

Phases $YbZn_{1-x}Al_x$, $YbZn_{2-x}Al_x$ and $YbZn_{3-x}Al_x$ were studied by electron microprobe analysis and X-ray single crystal and powder methods. The compound $YbZn_{0.8}Al_{0.2}$ crystallizes with the CsCl-type, $a = 3.635(2)$ Å. Four phases were investigated by single crystal X-ray diffraction: $YbZn_{0.996(6)}Al_{1.004(6)}$, $MgNi_2$-type, $P6_3/mmc$, $a = 5.573(1)$, $c = 18.051(3)$ Å, $Z = 8$, w$R2 = 0.040$ and $YbZn_{0.88(3)}Al_{1.12(3)}$, $MgCu_2$-type, $Fd\bar{3}m$, $a = 7.860(2)$ Å, $Z = 8$, w$R2 = 0.060$, both showing mixed Zn/Al occupancy; $YbZn_{2.50(1)}Al_{0.50(1)}$, $CeNi_3$-type, $P6_3/mmc$, $a = 5.496(1)$, $c = 17.336(2)$ Å, $Z = 6$, w$R2 = 0.036$ and $YbZn_{1.92(2)}Al_{1.08(2)}$, $PuNi_3$- or $NbBe_3$-type, $R\bar{3}m$, $a = 5.499(1)$, $c = 26.134(5)$ Å, $Z = 9$, w$R2 = 0.053$, where the zinc atoms are ordered in the $CaCu_5$ segment, while share the sites with aluminium in the Laves phase segment. In the pseudobinary section $YbZn_{2-x}Al_x$ four structures occur in sequence with increasing the electron concentration: $CeCu_2$ or KHg_2 ($x = 0$–0.3), $MgZn_2$ ($x = 0.33$–0.54), $MgNi_2$ ($x = 0.68$–1.01) and $MgCu_2$ ($x = 1.12$–2). This sequence agrees with the results of first-principles calculations, already reported in the literature for other similar series. In the $YbZn_{3-x}Al_x$ section $CeNi_3$-type compounds occur with $x = 0.40$–0.88 followed by $PuNi_3$-type compounds with $x = 0.92$–1.10. The stability ranges of these phases are related to the valence electron concentration.

1. Introduction

Several regions of the Yb–Zn–Al system were studied in previous papers [1–3]. The attention was then directed to the most frequent compositions occurring in the rare earth binary intermetallic phases, namely 1:2, 1:1 and 1:3, in the order. In the rare earth ternary systems too the largest number of compounds (about 1000) is found for the 1:1:1 composition, which is the counterpart of 1:2 when two partner elements contribute in equal ratio [4].

The $YbZn_{2-x}Al_x$ section ($0 \le x \le 2$) has $YbZn_2$ ($CeCu_2$- or KHg_2-type) [5] and $YbAl_2$ ($MgCu_2$-type) ([6] and Ref. therein) as end terms. Several series containing a dialuminide of Ca, Yb or Sr have been studied: $CaM_{2-x}Al_x$ with $M =$ Li [7], Mg [8], Ag [9,10], Zn [10–13], $YbAg_{2-x}Al_x$ [9,14] and $SrMg_{2-x}Al_x$ [15]. In all systems a sequence of Laves phase structures is present with more or less large stability ranges. In $CaLi_{2-x}Al_x$ [7], $CaMg_{2-x}Al_x$ [8] and $SrMg_{2-x}Al_x$ [15] chemical bonding and structural competition among the structure types are discussed in terms of first-principles calculations.

For the $YbZn_{3-x}Al_x$ section we can recall the investigation of the $R(Ag,Al)_3$ compounds with $R =$ Ca, Yb, Ce, Pr [9]. It is interesting to note that, notwithstanding the absence of "$YbAg_3$", "$CeAg_3$", "$PrAg_3$" and both "$CaAg_3$" and "$CaAl_3$" in the respective binary systems, this composition is stabilized by mixing Ag and Al elements, giving rise to phases with $CeNi_3$ and $PuNi_3$ (or $NbBe_3$) structure.

In order to compare the behaviour of Yb–Zn–Al with all these systems, in the present work we report on the pseudobinary section $YbZn_2$–$YbAl_2$ as well as the $YbZn_{0.8}Al_{0.2}$ and $Yb(Zn,Al)_3$ compounds.

2. Experimental

Nearly 20 samples were prepared from commercial metals with 99.9, 99.99 and 99.999 wt% purity, respectively, for ytterbium, zinc and aluminium and melted in Ta crucibles sealed by arc welding under pure argon. The alloys were annealed at 650–700 °C for 10–30 days and then air cooled. All samples were examined by both optical and scanning electron microscopy, and composition of the phases was determined by electron probe microanalysis (EPMA). X-ray analysis was carried out by powder and single-crystal methods. Powder patterns were obtained from a Guinier-Stoe camera with Cu$K\alpha$ radiation and Si as an internal standard ($a = 5.4308$ Å), and indexed by means of LAZY-PULVERIX

* Corresponding author. Fax: +39 010 3538733.
E-mail addresses: donata@chimica.unige.it (D. Mazzone), chimfis@chimica.unige.it (P. Manfrinetti), cfmet@chimica.unige.it (M.L. Fornasini).

0022-4596/$ - see front matter © 2009 Elsevier Inc. All rights reserved.
doi:10.1016/j.jssc.2009.06.012

[16]. Data of four single crystals were collected at room temperature on a Bruker-Nonius MACH3 diffractometer with graphite-monochromated Mo$K\alpha$ radiation and their lattice parameters calculated from 25 diffractometer-measured reflections at $\theta = 25$–29°. Main programs used: SIR97 [17] for structure solution, SHELXL-97 [18] for structure refinement, STRUCTURE TIDY [19] for atomic coordinates standardization. Details of the four single-crystal data collections and refinements are listed in Table 1. Further details of the crystal structure investigations may be obtained from Fachinformationszentrum Karlsruhe, 76344 Eggenstein-Leopoldshafen, Germany, fax: +49 7247 808 666; e-mail: crysdata@fiz-karlsruhe.de, on quoting the deposition numbers CSD-420509 ($YbZn_{0.88}Al_{1.12}$), CSD-420510 ($YbZn_{0.996}Al_{1.004}$), CSD-420511 ($YbZn_{2.50}Al_{0.50}$), CSD-420512 ($YbZn_{1.92}Al_{1.08}$).

3. Results and discussion

3.1. The $YbZn_{0.8}Al_{0.2}$ phase

The YbZn compound crystallizes with the cubic CsCl structure, $a = 3.629(3)$ Å [20], while no "YbAl" phase is formed. A replacement of zinc by the larger aluminium atoms resulted in a solid solubility range up to the $YbZn_{0.80(3)}Al_{0.20(3)}$ composition with lattice parameter $a = 3.635(2)$ Å.

3.2. The pseudobinary section $YbZn_{2-x}Al_x$

In the pseudobinary section $YbZn_{2-x}Al_x$ four structures are found on increasing the aluminium content from $x = 0$ to 2. Combining the results of the electron probe microanalysis and the X-ray powder patterns interpretation it was possible to define the existence range for each structure type. Starting from $YbZn_2$ ($x = 0$) with $CeCu_2$-type [5], this structure is maintained up to 10 at% Al, then the three Laves phases $MgZn_2$, $MgNi_2$ and $MgCu_2$ occur in sequence, in the ranges 11–18, 23–34 and 37–66.7 at% Al, respectively, being closed by the known $YbAl_2$ phase ($MgCu_2$-type, $x = 2$) [6]. The estimated uncertainty for the homogeneity ranges is 1.0–1.5 at%. Table 2 lists the structure type and lattice parameters of the examined phases as obtained by Guinier powder patterns.

Single crystals picked out in alloys with nominal composition YbZnAl and $YbZn_{0.88}Al_{1.12}$ were found to crystallize with different Laves phase structures, confirming their initial composition. The phase $YbZn_{0.996(6)}Al_{1.004(6)}$ belongs to the $MgNi_2$-type with mixed Zn/Al occupancy of the three sites, while $YbZn_{0.88(3)}Al_{1.12(3)}$ has $MgCu_2$-type structure. The atomic parameters of the two compounds are reported in Table 3, while interatomic distances are available as supplementary material. No single crystals suitable for X-ray analysis could be found for the ternary phases with $CeCu_2$ and $MgZn_2$ structures, because the samples were always microcrystalline.

Table 1
Crystal data of the four single crystals examined.

	$YbZn_{0.996(6)}Al_{1.004(6)}$	$YbZn_{0.88(3)}Al_{1.12(3)}$	$YbZn_{2.50(1)}Al_{0.50(1)}$	$YbZn_{1.92(2)}Al_{1.08(2)}$
Crystal system, Z	Hexagonal, 8	Cubic, 8	Hexagonal, 6	Trigonal, 9
Space group	$P6_3/mmc$ (no. 194)	$Fd\bar{3}m$ (no. 227)	$P6_3/mmc$ (no. 194)	$R\bar{3}m$ (no. 166)
a (Å)	5.573(1)	7.860(2)	5.496(1)	5.499(1)
c (Å)	18.051(3)		17.336(2)	26.134(5)
Cell volume, formula weight	485.5(2), 265.2	485.6(2), 260.8	453.5(1), 350.0	684.4(2), 327.7
Scan mode, θ range (deg)	ω–θ, 2–30	ω–2θ, 2–35	ω–θ, 2–30	ω–θ, 2–30
Range in h,k,l	±7; 0+7; ±25 with $\lvert h\rvert > \lvert k\rvert$	±12; 0+12; 0+12	±7; 0+7; ±24 with $\lvert h\rvert > \lvert k\rvert$	±7; ±7; ±36
Total number of reflections	1873	591	1763	2632
Single crystal sizes (mm)	0.03 × 0.07 × 0.08	0.04 × 0.05 × 0.08	0.06 × 0.09 × 0.10	0.015 × 0.065 × 0.08
Absorption coefficient (mm^{-1})	48.1	47.0	50.1	45.5
Absorption correction method	Psi-scan	Psi-scan	Psi-scan	Gaussian integration
Independent refl., R_{int} (F_o^2)	315, 0.095	70, 0.067	297, 0.079	289, 0.037
Reflections with $F_o > 4\sigma$ (F_o)	215	64	238	251
Number of parameters	22	5	21	19
Extinction coefficient	0.0028(2)	–	0.0044(2)	–
$wR(F_o^2)$, all data	0.040	0.060	0.036	0.053
R [$F_o > 4\sigma(F_o)$]	0.017	0.023	0.017	0.021
Goodness of fit (S)	0.846	1.216	0.930	1.008
$\Delta\rho_{min}$, $\Delta\rho_{max}$ (e Å^{-3})	−1.45, 0.97	−2.62, 1.58	−1.02, 1.14	−3.82, 0.98

Table 2
Structure type, lattice parameters and volume per atom in the $YbZn_{2-x}Al_x$ phases.

Phase	Structure type	Pearson code	a (Å)	b (Å)	c (Å)	V_{at} (Å^3)
$YbZn_2$ [5]	$CeCu_2$	*oI*12	4.573(4)	7.325(7)	7.569(7)	21.13(3)
$YbZn_{1.70}Al_{0.30}$			4.548(1)	7.266(2)	7.680(3)	21.15(1)
$YbZn_{1.67}Al_{0.33}$	$MgZn_2$	*hP*12	5.600(2)		8.847(4)	20.02(1)
$YbZn_{1.46}Al_{0.54}$			5.6081(7)		8.856(1)	20.102(4)
$YbZn_{1.32}Al_{0.68}$	$MgNi_2$	*hP*24	5.5660(6)		18.048(2)	20.186(4)
$YbZn_{1.14}Al_{0.86}$			5.5676(6)		18.049(3)	20.189(5)
$YbZn_{0.99}Al_{1.01}$			5.576(1)		18.062(2)	20.265(5)
$YbZn_{0.88}Al_{1.12}$	$MgCu_2$	*cF*24	7.865(3)			20.27(1)
$YbZn_{0.57}Al_{1.43}$			7.872(4)			20.33(2)
$YbZn_{0.24}Al_{1.76}$			7.877(2)			20.365(9)
$YbAl_2$ [6]			7.881			20.40

V_{at} is the cell volume divided by the total number of atoms.

Table 3
Atomic coordinates and equivalent isotropic displacement parameters of $YbZn_{0.996(6)}Al_{1.004(6)}$ ($MgNi_2$-type) and $YbZn_{0.88(3)}Al_{1.12(3)}$ ($MgCu_2$-type).

Atom	Site	Occupancy	x	y	z	U_{eq} (Å^2)
$YbZn_{0.996(6)}Al_{1.004(6)}$	(space group $P6_3/mmc$)					
Yb1	4*f*	1	1/3	2/3	0.65609(3)	0.0067(2)
Yb2	4*e*	1	0	0	0.09335(4)	0.0068(2)
Zn1/Al	6*h*	0.613(7)/0.387	0.1630(2)	0.3260(4)	1/4	0.0092(5)
Zn2/Al	6*g*	0.447(8)/0.553	1/2	0	0	0.0077(6)
Zn3/Al	4*f*	0.402(11)/0.598	1/3	2/3	0.1286(2)	0.0074(7)
$YbZn_{0.88(3)}Al_{1.12(3)}$	(space group $Fd\bar{3}m$, origin at centre)					
Yb	8*b*	1	3/8	3/8	3/8	0.0076(3)
Zn/Al	16*c*	0.438(15)/0.562	0	0	0	0.0093(7)

U_{eq} is defined as one third of the trace of the orthogonalized U_{ij} tensor.

Fig. 1 shows the picture of Laves phase structures occurring in the $YbZn_{2-x}Al_x$ system. The majority atoms form tetrahedra sharing vertices in the $MgCu_2$-type and columns of trigonal bipyramids in the $MgZn_2$-type. The $MgNi_2$ structure, which is described as an intergrowth of the two mentioned structures, shows both vertex-sharing tetrahedra and bipyramids.

As already observed for other compounds crystallizing with the $MgNi_2$-type in the systems $CaMg_{2-x}Al_x$ [8] and $CaZn_{2-x}Al_x$ [10–13], also for $YbZn_{0.996}Al_{1.004}$ two characteristic aspects can be mentioned regarding the 6*h* site $(x, 2x, \frac{1}{4})$: a preferential occupation by the more electronegative element and a decreasing of the x parameter from the ideal value 0.1667, causing a distortion of the corresponding kagomé net. In this case the x parameter decreases to 0.1630 in the 6*h* site (Zn1/Al) mainly filled with zinc, allowing to realize a close Zn1/Al–2Yb2 contact of 3.236(1) Å, while maintaining the similar Zn1/Al–4Yb1 distance of 3.262(1) Å, which is practically insensible to the change of the x parameter. The trend of the Zn/Al–Zn/Al distances in $YbZn_{0.996}Al_{1.004}$ is related to the occupation of the three mixed Zn/Al sites. The distances increase by replacing more zinc with the larger aluminium. The Zn1/Al atom (6*h*), with an occupation of 61% by Zn, shows a mean radius of 1.363 Å, half of the shortest Zn1/Al–Zn1/Al distance, while the radius of Zn2/Al (6*g*) is 1.393 Å against a Zn filling of 45%. The mean radius of the apical Zn3/Al (4*f*), obtained as difference from its distances to the other two Zn/Al atoms, is 1.404 Å for the lowest Zn content of 40%. The same holds in phases crystallizing with the $MgNi_2$-type in the Ca–Zn–Al system and showing mixed occupancies too [10].

The atomic volumes of the $YbZn_{2-x}Al_x$ phases vs. composition are shown in Fig. 2. The plot shows a sharp decrease of the atomic volume (5%) on going from the $CeCu_2$-type to Laves phases. The following smooth increase is simply due to the replacement of zinc with the larger aluminium atoms. A very similar trend is found, for instance, in the $CaZn_{2-x}Al_x$ [10,12] and $CaAg_{2-x}Al_x$ [10] systems, where the transition from $CeCu_2$ to $MgNi_2$ occurs with 4% and 6% decrease of the volume per atom, respectively. The observed behaviour can be related to the greater compression of the Yb–Yb or Ca–Ca contacts. In fact, in $YbZn_2$ ($CeCu_2$-type) [5] the mean Yb–Yb distance is 3.77 Å, but short Yb–Yb distances, typical of Laves phase structures, are found for $YbZn_{0.996(6)}Al_{1.004(6)}$ ranging from 3.370(1) to 3.411(1) Å, and for $YbZn_{0.88(3)}Al_{1.12(3)}$ with 3.404(1) Å. The same is observed for the other two cited systems. The mean Ca–Ca distance decreases from 3.78 Å in $CaZn_2$ ($CeCu_2$-type) to 3.46 Å in $CaZn_{0.594}Al_{1.406}$ ($MgNi_2$-type) and from 3.89 Å in $CaAg_2$ ($CeCu_2$-type) to 3.48 Å in CaAgAl ($MgZn_2$-type) [10].

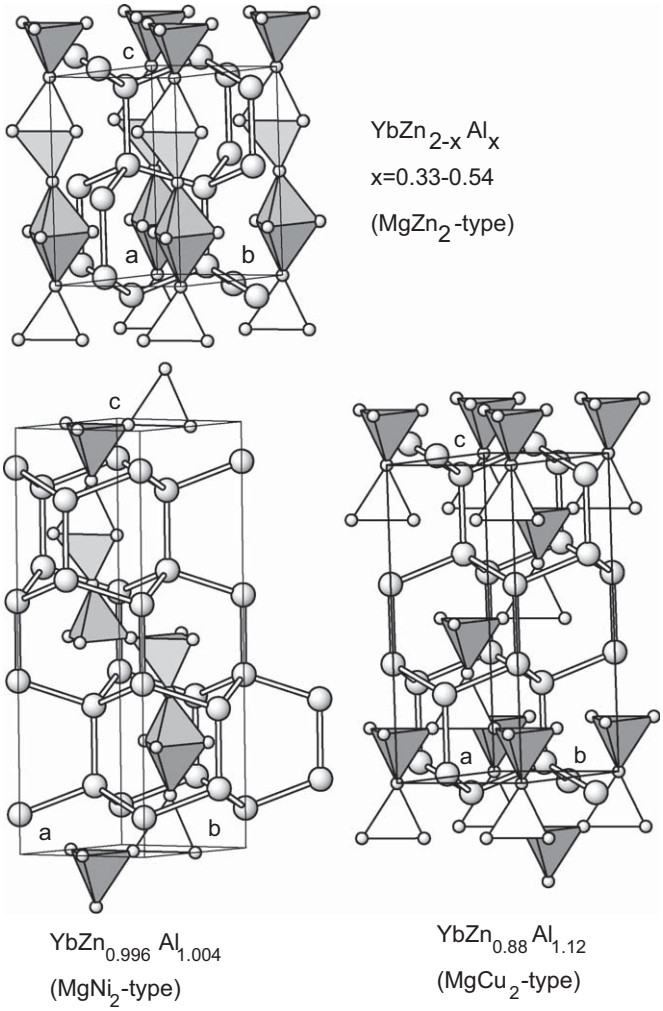

Fig. 1. Laves phase structures in the $YbZn_{2-x}Al_x$ section. The $YbZn_{0.88}Al_{1.12}$ compound ($MgCu_2$-type) is referred to a rhombohedral cell with hexagonal axes. Large circles: Yb; small circles: Zn/Al. Tetrahedra formed by Zn/Al atoms are highlighted.

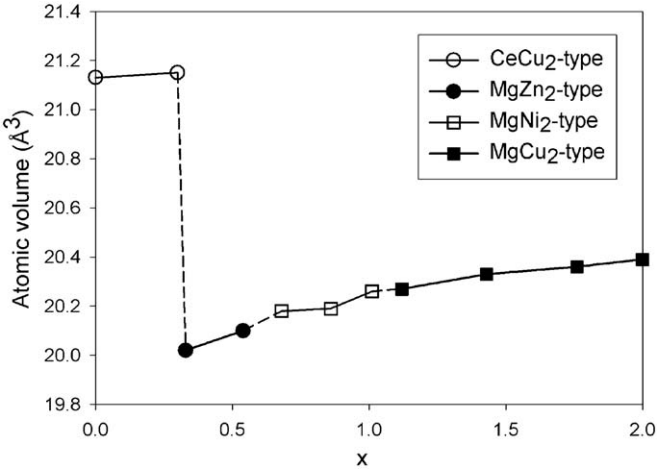

Fig. 2. Atomic volumes vs. composition in the $YbZn_{2-x}Al_x$ phases. The errors are within the symbol size.

As it was recently pointed out in the study of the $CaAg_2$–$CaZn_2$–$CaAl_2$ pseudo ternary system [10], in these AB_2 phases the maximum space filling, i.e. the contemporaneous occurrence of

A–A, B–B and A–B contacts, is realized at an ideal ratio $r_A/r_B = 1.225$ for the Laves phases, but at the greater value of 1.39–1.47 for the $CeCu_2$-type compounds. If the radius ratio is evaluated using the experimental A–A and B–B distances, all Laves phase compounds are very near to have the ideal ratio, as reported by Dwight for a large number of phases [21] and confirmed also by the Laves phase compounds of the present work. On the other hand, the small contraction in the A–A distances of the $CeCu_2$-type compounds gives rise to higher r_A/r_B values, again very near to the ideal ratio. First-principles density functional calculations were used to investigate the structural competition between Laves phase types and $CeCu_2$ in alkaline earth dialuminides [15]. It was found that, increasing the alkaline earth size, Laves phase structures are destabilized going from $CaAl_2$ ($MgCu_2$-type) to $SrAl_2$ ($CeCu_2$-type). At the same time shorter Al–Al contacts are realized by this transition, reaching a higher r_A/r_B ratio.

We can now compare the stability range for the different structure types occurring in the $YbZn_{2-x}Al_x$ system and in six other pseudobinary systems where Laves phase structures are formed. On increasing the valence electron concentration (VEC), i.e. increasing the aluminium content, the sequence $MgZn_2$ (C14)–$MgNi_2$ (C36)–$MgCu_2$ (C15) is always found in the $CaLi_{2-x}Al_x$ [7], $CaMg_{2-x}Al_x$ [8], $CaAg_{2-x}Al_x$ [10] and $YbZn_{2-x}Al_x$ systems. In other cases a Laves phase structure is lacking, but the sequence keeps its validity on increasing the valence electron concentration: $MgZn_2$–$MgNi_2$ for $SrMg_{2-x}Al_x$ [15], $MgZn_2$–$MgCu_2$ for $YbAg_{2-x}Al_x$ [9,14] and $MgNi_2$–$MgCu_2$ for $CaZn_{2-x}Al_x$ [10–13]. In five systems a binary term, namely $SrAl_2$, $CaAg_2$, $CaZn_2$, $YbAg_2$ or $YbZn_2$, belongs to the orthorhombic $CeCu_2$-type. The phase width for this structure is generally limited, but for the $CaZn_{2-x}Al_x$ system it extends up to $x = 1.07$ [12], as in this system the $MgZn_2$-type is lacking.

The moments method applied to Hückel-based tight binding theory [22] was used to explain the structural trend $MgCu_2 \rightarrow MgNi_2 \rightarrow MgZn_2$ with decreasing electron concentration in *s–p* systems, such as $CaMg_{2-x}Al_x$ [8]. Differently from the $MgCu_2$ structure, in calculating the fourth moment for the $MgNi_2$ and $MgZn_2$ structures an additional contribution comes from the four-membered rings present in the trigonal bipyramids of the majority atoms. Thus, the fourth moment increases going from $MgCu_2$ to $MgNi_2$ to $MgZn_2$, stabilizing the structure at lower band filling and then at lower electron concentration [8].

3.3. The $YbZn_{3-x}Al_x$ phases

In the Yb–Zn system the "$YbZn_3$" phase does not exist. However, the addition of aluminium for zinc stabilizes a phase with composition ranging from $YbZn_{2.6}Al_{0.4}$ (10 at% Al) to $YbZn_{2.12}Al_{0.88}$ (22 at% Al) with hexagonal $CeNi_3$ structure. Increasing the Al content the rhombohedral $PuNi_3$ structure appears in phases with composition 23–27 at% Al. The estimated uncertainty for the homogeneity ranges is 1.0–1.5 at%. Table 4 shows the lattice parameters of the phases delimiting the existence ranges of the $YbZn_{3-x}Al_x$ phases.

Single crystals were isolated from the alloys $YbZn_{2.6}Al_{0.4}$ annealed at 700 °C for seven days and $YbZn_2Al$ annealed at 680 °C for five days. The refinement of their structure gave the compositions $YbZn_{2.50(1)}Al_{0.50(1)}$ ($CeNi_3$-type) and $YbZn_{1.92(2)}Al_{1.08(2)}$ ($PuNi_3$-type), respectively. The atomic parameters are listed in Table 5, while interatomic distances are available as supplementary material.

It is known that the $CeNi_3$- and $PuNi_3$-types are formed by linear intergrowth along the *c* axis of $MgZn_2$–$CaCu_5$ and $MgCu_2$–$CaCu_5$ blocks, respectively [23]. A picture of the two structures is shown in Fig. 3. Pairs of vertex joined tetrahedra of Zn/Al atoms occur in the Laves phase slab, alternated with the $CaCu_5$ slab where the Yb2 atom of both structures is surrounded by the typical CN20 polyhedron, a hexagonal prism capped on all faces. The kagomé nets formed by atoms in 12*k* ($CeNi_3$) or 18*h* ($PuNi_3$) represent the boundary between the different slabs. In both examined crystals the Zn atoms are ordered inside the $CaCu_5$ segment, where their coordination (CN9) is lower than in the other two sites (CN12), due to a smaller number of Yb–Zn contacts. The Al atoms share their sites with zinc, showing a preferential occupation for the sites in the Laves phase segment. As already observed for the $YbZn_{2-x}Al_x$ structures, short Yb1–Yb1 distances are present in the Laves phase segment, with 3.386(1) and 3.406(1) Å for the $CeNi_3$- and $PuNi_3$-type compounds, respectively, while larger distances connect the Yb1 and Yb2 atoms through different segments (3.743(1) and 3.739(1) Å, respectively).

Starting from the parent $CeNi_3$ and $PuNi_3$-types several ternary structures were derived with an ordered or partially ordered filling of the Ni sites by a transition element and an *s–p* element: Ce_3Co_8Si [24], $Dy_3Ni_7B_2$ [24], $Ca_3Cu_2Al_7$ [25] and $YRhSi_2$ [26] can be cited as examples. Moreover, part of the electropositive Ce or Pu elements can be replaced by Mg, giving rise to two ordered structures, as reported for the series RCu_9Mg_2 ($CeNi_3$ derived) [27] and RNi_9Mg_2 ($PuNi_3$ derived) [28] with *R* = rare earth.

Noticeable similarities can be pointed out by comparing the phases of the present work with the phases $YbAg_{1.3}Al_{1.7}$ and $CaAg_{1.3}Al_{1.7}$ (both $CeNi_3$-type) and $YbAg_{0.7}Al_{2.3}$, $CaAg_{0.7}Al_{2.3}$, $CeAg_{0.9}Al_{2.1}$ and $PrAgAl_2$ (all $PuNi_3$-type) studied by Cordier et al. [9]. (i) The Ag atoms (like Zn) are always ordered inside the $CaCu_5$ segment, while aluminium atoms preferentially occupy the two other available sites, sometimes in an ordered way. (ii) The sequence $CeNi_3$–$PuNi_3$ is observed (like in the Yb–Zn–Al system) on increasing the valence electron concentration. (iii) The

Table 4
Structure type, lattice parameters and volume per atom in the $YbZn_{3-x}Al_x$ phases.

Phase	Structure type	Pearson code	*a* (Å)	*c* (Å)	V_{at} (Å^3)
$YbZn_{2.60}Al_{0.40}$	$CeNi_3$	*hP*24	5.500(1)	17.343(2)	18.931(5)
$YbZn_{2.12}Al_{0.88}$			5.5154(6)	17.339(3)	19.033(5)
$YbZn_{2.08}Al_{0.92}$	$PuNi_3$	*hR*36	5.500(3)	26.17(2)	19.04(1)
$YbZn_{1.90}Al_{1.10}$			5.508(1)	26.149(5)	19.084(6)

V_{at} is the cell volume divided by the total number of atoms.

Table 5
Atomic coordinates and equivalent isotropic displacement parameters of $YbZn_{2.50(1)}Al_{0.50(1)}$ ($CeNi_3$-type) and $YbZn_{1.92(2)}Al_{1.08(2)}$ ($PuNi_3$-type).

Atom	Site	Occupancy	*x*	*y*	*z*	U_{eq} (Å^2)
$YbZn_{2.50(1)}Al_{0.50(1)}$ (space group $P6_3/mmc$)						
Yb1	4*f*	1	1/3	2/3	0.53409(3)	0.0081(2)
Yb2	2*d*	1	1/3	2/3	3/4	0.0115(2)
Zn1	2*c*	1	1/3	2/3	1/4	0.0139(4)
Zn2	2*b*	1	0	0	1/4	0.0124(4)
Zn3/Al	12*k*	0.827(5)/0.173	0.16797(11)	0.33594(22)	0.12684(4)	0.0105(3)
Zn4/Al	2*a*	0.552(10)/0.448	0	0	0	0.0103(7)
$YbZn_{1.92(2)}Al_{1.08(2)}$ (space group $R\bar{3}m$)						
Yb1	6*c*	1	0	0	0.14308(3)	0.0067(2)
Yb2	3*a*	1	0	0	0	0.0109(2)
Zn1	6*c*	1	0	0	0.33495(7)	0.0134(4)
Zn2/Al	18*h*	0.594(8)/0.406	0.50305(13)	0.49695(13)	0.08222(5)	0.0091(4)
Zn3/Al	3*b*	0.183(19)/0.817	0	0	1/2	0.0054(14)

U_{eq} is defined as one third of the trace of the orthogonalized U_{ij} tensor.

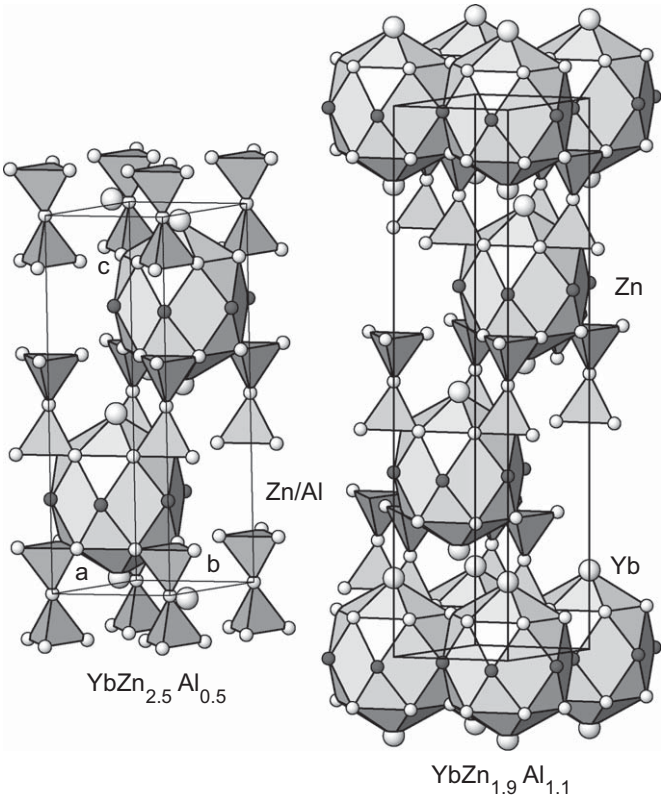

Fig. 3. The unit cells of $YbZn_{2.5}Al_{0.5}$ ($CeNi_3$-type) and $YbZn_{1.9}Al_{1.1}$ ($PuNi_3$-type). The CN20 polyhedron around Yb2 in the $CaCu_5$ segment and the Zn/Al tetrahedra in the Laves phase segment of both structures are highlighted.

$CeNi_3$- and $PuNi_3$-type compounds are formed in a range (43–58 at% Al) greater than in the Yb–Zn–Al system (10–28 at% Al). However, using the VEC values and considering ytterbium as a divalent element, we find similar ranges: 2.1–2.5 e/atom for the *R*–Ag–Al systems (*R* = Ca, Yb, Ce, Pr) and 2.1–2.3 e/atom for the Yb–Zn–Al system.

3.4. The Yb–Zn–Al system

A view of the 14 phases studied in the Yb–Zn–Al system is shown in Fig. 4 [1–3]. The compounds studied in the present work are identified by their structure types, all others by numbers.

Two further compounds taken from the literature are added: $YbZn_{1.65}Al_{2.35}$ ($BaAl_4$-type) [29] (phase 3), and $Yb_8Zn_{40.6}Al_{25.4}$ ($Yb_8Cu_{17}Al_{49}$-type) [30] (phase 5), representing the composition limit of this phase on the Al-rich side.

Some binary compounds on the Zn-rich side show more or less extended solubility fields in the ternary system. This occurs with phases crystallizing with the CsCl, $CeCu_2$, La_3Al_{11} (phase 1) and $YbZn_6$ (phase 4) types. Starting from Yb_3Zn_{11} with La_3Al_{11} structure, a replacement of only 3 at% Al for Zn is reached, then a heterogeneity range appears. The phase becomes again stable with a larger aluminium content between 35 and 50 at% Al (phase 2). On the Al-rich side extended solid solubility is obtained starting from $YbAl_2$ and replacing aluminium up to 30 at% Zn. On the whole the $YbZn_{2-x}Al_x$ section shows the sequence of structures $CeCu_2$–$MgZn_2$–$MgNi_2$–$MgCu_2$ on increasing the aluminium content.

The phases labelled 6, 7, 8, 9, localized in the zinc-rich corner between 71 and 85 at% Zn, are not present in the Yb–Zn system,

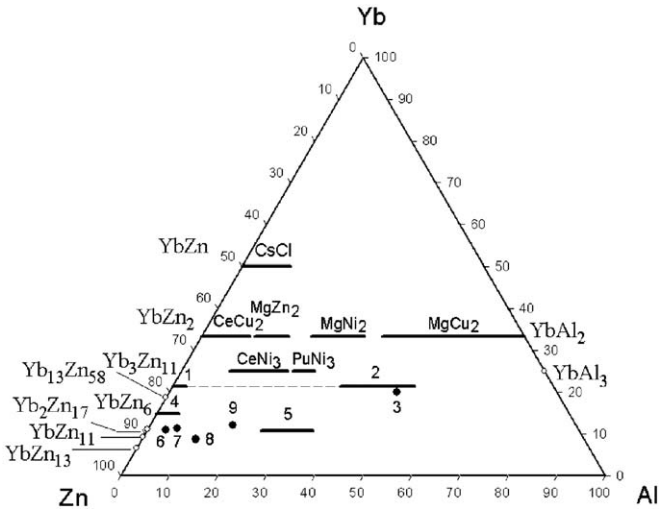

Fig. 4. Phases stable at 650–700 °C in the Yb–Zn–Al system. Structure types show compounds studied in the present work. Numbers show compounds in the literature. 1+2 = $Yb_3(Zn,Al)_{11}$ (La_3Al_{11}-type) [2]; 3 = $YbZn_{1.65}Al_{2.35}$ ($BaAl_4$-type) [29]; 4 = $Yb(Zn,Al)_6$ (YCd_6-type) [3]; 5 = $Yb_8(Zn,Al)_{66}$ ($Yb_8Cu_{17}Al_{49}$-type) [2,30]; 6 = $Yb_{12.4}Zn_{96.8}Al_{4.4}$ (U_2Zn_{17}-type) [1]; 7 = $Yb_{6.4}Zn_{46.8}Al_{3.4}$ [1]; 8 = $Yb_{3.36}Zn_{30.94}Al_{4.34}$ ($SmZn_{11-x}$-type) [1]; 9 = $Yb_3Zn_{17.7}Al_{4.3}$ (Ce_3Zn_{22}-type) [1].

but are stabilized as ternary phases by the introduction of aluminium atoms. They belong to the large family of structures derived from the $CaCu_5$-type, where some ytterbium atoms are totally or partially replaced by dumbbells of Zn/Al atoms, giving rise to cells multiple of the parent one. Notwithstanding the disorder, the zinc atoms occupy several sites in an ordered way, as it is expected for Zn-rich compounds. The percentage of ordered Zn-filled sites over the total available for Zn and Al atoms is 70%, 67%, 50% and 20% for the four phases 6, 7, 8, 9.

Ordering of the Zn atoms in two of six sites is also found in two compounds (phase 5) with a structure similar to $Yb_8Cu_{17}Al_{49}$, but with a Zn:Al ratio reversed with respect to the prototype. In $CeNi_3$- and $PuNi_3$-type phases the zinc atoms fill ordered sites only in the $CaCu_5$ segment of both structures, while in their Laves phase segments mixed Zn/Al occupancy occurs.

Appendix A. Supplementary material

Supplementary data associated with this article can be found in the online version at 10.1016/j.jssc.2009.06.012.

References

[1] M.L. Fornasini, P. Manfrinetti, D. Mazzone, J. Solid State Chem. 179 (2006) 2012–2019.
[2] M.L. Fornasini, P. Manfrinetti, D. Mazzone, Intermetallics 15 (2007) 856–861.
[3] M.L. Fornasini, P. Manfrinetti, D. Mazzone, S.K. Dhar, Z. Naturforsch. B 63 (2008) 237–243.
[4] M.L. Fornasini, F. Merlo, M. Pani, in: J.H. Westbrook, R.L. Fleischer (Eds.), Intermetallic Compounds: Principles and Practice, vol. 3, Wiley, Baffins Lane, Chichester, 2002, p. 85.
[5] D.J. Michel, E. Ryba, Acta Crystallogr. 19 (1965) 687–688.
[6] A. Palenzona, J. Less-Common Met. 29 (1972) 289–292.
[7] R. Nesper, G.J. Miller, J. Alloys Compd. 197 (1993) 109–121.
[8] S. Amerioun, S.I. Simak, U. Häussermann, Inorg. Chem. 42 (2003) 1467–1474.
[9] G. Cordier, E. Czech, G. Dörsam, R. Henseleit, C. Röhr, A. Mehner, S. Thies, C. Geibel, J. Less-Common Met. 169 (1991) 55–72.
[10] M. Pani, M.L. Fornasini, F. Merlo, Z. Kristallogr. 222 (2007) 218–225.
[11] T. Yokosawa, K. Söderberg, M. Boström, D. Grüner, G. Kreiner, O. Terasaki, Z. Kristallogr. 221 (2006) 357–374.

[12] K. Söderberg, M. Boström, Y. Kubota, T. Nishimatsu, R. Niewa, U. Häussermann, Y. Grin, O. Terasaki, J. Solid State Chem. 179 (2006) 2690–2697.
[13] K. Söderberg, Y. Kubota, N. Muroyama, D. Grüner, A. Yoshimura, O. Terasaki, J. Solid State Chem. 181 (2008) 1998–2005.
[14] M.L. Fornasini, A. Iandelli, F. Merlo, M. Pani, Intermetallics 8 (2000) 239–246.
[15] S. Amerioun, T. Yokosawa, S. Lidin, U. Häussermann, Inorg. Chem. 43 (2004) 4751–4760.
[16] K. Yvon, W. Jeitschko, E. Parthé, J. Appl. Crystallogr. 10 (1977) 73–74.
[17] A. Altomare, M.C. Burla, M. Camalli, G.L. Cascarano, C. Giacovazzo, A. Guagliardi, A.G.G. Moliterni, G. Polidori, R. Spagna, J. Appl. Crystallogr. 32 (1999) 115–119.
[18] G.M. Sheldrick, SHELXL-97, Program for the Refinement of Crystal Structures, University of Göttingen, Göttingen, Germany, 1997.
[19] L.M. Gelato, E. Parthé, J. Appl. Crystallogr. 20 (1987) 139–143.
[20] A. Iandelli, A. Palenzona, J. Less-Common Met. 9 (1965) 1–6.
[21] A.E. Dwight, Trans. ASM 53 (1961) 479–500.
[22] J.K. Burdett, S. Lee, J. Am. Chem. Soc. 107 (1985) 3050–3063 and 3063–3082.
[23] E. Parthé, R. Lemaire, Acta Crystallogr. B 31 (1975) 1879–1889.
[24] E. Parthé, B. Chabot, in: K.A. Gschneidner Jr., L. Eyring (Eds.), Handbook on the Physics and Chemistry of Rare Earths, vol. 6, Elsevier, Amsterdam, 1984, p. 113.
[25] G. Cordier, E. Czech, H. Ochmann, H. Schäfer, J. Less-Common Met. 99 (1984) 173–185.
[26] L. Paccard, D. Paccard, J. Less-Common Met. 109 (1985) 229–232.
[27] P. Solokha, V. Pavlyuk, A. Saccone, S. De Negri, W. Prochwicz, B. Marciniak, E. Różycka-Sokołowska, J. Solid State Chem. 179 (2006) 3073–3081.
[28] K. Kadir, T. Sakai, I. Uehara, J. Alloys Compd. 257 (1997) 115–121.
[29] B. Stel'makhovych, O. Stel'makhovych, Yu. Kuz'ma, J. Alloys Compd. 397 (2005) 115–119.
[30] O. Stel'makhovych, Yu. Kuz'ma, Z. Naturforsch. B 61 (2006) 779–784.